Whole human heart histology to validate electroanatomical voltage mapping in patients with non-ischemic cardiomyopathy and ventricular tachycardia

C.A. Glashan, MD[1]; A.F.A. Androulakis, MD[1]; Q. Tao, PhD[2]; R.N. Glashan; L. Wisse[3]; M. Ebert, MD[1]; M.C. de Ruiter, PhD[3]; B.J. van Meer[3]; C. Brouwer, MD[1]; O. M. Dekkers, MD, PhD[4]; D.A. Pijnappels, PhD[1]; J.M.T. de Bakker, PhD[5]; M. de Riva, MD[1]; S.R.D Piers, MD, PhD[1]; K. Zeppenfeld, MD, PhD[1]

1. Department of Cardiology, Leiden University Medical Centre, Leiden, The Netherlands
2. LKEB–Division of Image Processing, Department of Radiology, Leiden University Medical Centre, Leiden, The Netherlands
3. Department of Anatomy and Embryology, Leiden University Medical Centre, Leiden, The Netherlands
4. Department of Epidemiology, Leiden University Medical Center, Leiden, The Netherlands
5. Department of Clinical and Experimental Cardiology, Academic Medical Centre, Amsterdam, The Netherlands

Corresponding author:

K. Zeppenfeld, MD, PhD

Telephone: +31715262020

K.Zeppenfeld@lumc.nl

Word count: 3920

Abstract

Aims

Electroanatomical voltage mapping (EAVM) is an important diagnostic tool for fibrosis identification and risk stratification in non-ischemic cardiomyopathy (NICM); currently distinct cut-offs are applied. We aimed to evaluate the performance of EAVM to detect fibrosis by integration with whole heart histology and to identify the fibrosis pattern in NICM patients with ventricular tachycardias (VT).

Methods and Results

Eight patients with NICM and VT underwent EAVM prior to death or heart transplantation. EAVM data was projected onto slices of the entire heart. Pattern, architecture and amount of fibrosis was assessed in transmural biopsies corresponding to EAVM sites. Fibrosis pattern in NICM biopsies (n=507) was highly variable and not limited to mid-wall/sub-epicardium. Fibrosis architecture was rarely compact, but typically patchy and/or diffuse. In NICM biopsies without abnormal fibrosis unipolar (UV) and bipolar (BV) voltages showed a linear association with wall thickness (WT). The amount of viable myocardium showed a linear association with both UV and BV. Accordingly, any cut-off to delineate fibrosis performed poorly. An equation was generated calculating the amount of fibrosis at any location, given WT and UV or BV.

Conclusion

Considering the linear relationships between WT, amount of fibrosis and both UV and BV, the search for any distinct voltage cut-off to identify fibrosis in NICM is futile. The amount of fibrosis can be calculated if WT and voltages are known. Fibrosis pattern and architecture are different from ischemic cardiomyopathy and findings on ischemic substrates may not be applicable to NICM.

Key words

Arrhythmias, Mapping, Histology, Fibrosis, Cardiomyopathy

Introduction

Sustained ventricular tachycardia (VT) in patients with non-ischemic cardiomyopathy (NICM) is often due to myocardial re-entry and occasionally to triggered activity both associated with the presence of fibrosis[1, 2]. Animal models and human data in end-stage heart failure suggest that the degree of arrhythmogeneity depends on amount and architecture of fibrosis with highest propensity for intermediate degrees and patchy architecture[3-5]. However, histological data from patients with NICM and sustained monomorphic VT (MVT) is lacking.

Electroanatomical bipolar (BV) and unipolar voltage (UV) mapping is considered an invasive reference method to detect fibrosis[6]. Different endocardial BV and UV cut-off values for detecting fibrosis have been proposed[7-9]. It has been suggested that the presence of a viable sub-endocardial layer overlying fibrosis may prevent its detection by BV mapping using the currently uniformly applied BV cut-off of 1.5mV[8, 9]. UV mapping is considered to have a larger field of view and thus superior in detecting mid-wall and sub-epicardial fibrosis[9-11]. However, neither the currently used cut-off values for detecting fibrosis in NICM, nor the "field of view" of UV or BV have been validated. To date, the only histological validation of electroanatomical voltage mapping (EAVM) for scar detection arises from animal infarct models[12]. Infarct scars, with a transmural pattern and compact fibrosis interspersed with viable myocardial bundles, may be substantially different from NICM scars[4, 13]. Animal models mimicking NICM scar patterns are lacking.

The purpose of this study was twofold: (1) to evaluate the location, pattern, architecture and amount of fibrosis in patients with NICM and sustained VT and (2) to evaluate the performance of EAVM to detect fibrosis by ex-vivo registration of EAVM data with whole heart histology.

Methods

Patients and Controls

NICM patients who underwent detailed EAVM and ablation for MVT and either died or received heart transplantation after the procedure were included (Supplementary data). All patients were treated according to our standard clinical protocol and provided informed consent for mapping and ablation. All patients and/or next of kin provided informed consent for post-mortem analysis.

Transmural biopsies from seven age-matched hearts, in which cardiac pathology was excluded by an experienced pathologist, served as controls.

Electroanatomical mapping and ablation

High-density EAVM was performed during sinus rhythm or RV pacing using a 3.5mm irrigated-tip catheter (1mm ring electrode, 2mm inter-electrode spacing; NaviStar Thermocool, Biosense Webster Inc., CA) and the CARTO system (figure 1A) (Supplementary data)[7, 11, 14, 15].

Ex-vivo image integration

Three-dimensional meshes were created from 5mm thick slices of the fixed heart, imported into CARTO, and merged with EAVM data (figure 1B-C) (Supplementary data)[9].

Histological analysis

Transmural biopsies (TB) with a width of 5mm (7µm thick) were taken from LV sites corresponding to non-ablation EAVM sites and stained with Picrosirius Red (Figure 1D) (Supplementary data). In all patients, TB were taken from seven locations: the anterior-septal, lateral and inferior wall at the mid and basal level and the apex. TB with signs of acute or old ablation lesions were excluded. TB were systematically assessed on the following parameters:

I) Location

The fibrotic involvement of the seven LV segments was macroscopically assessed in the stained TB to determine the location of fibrosis.

II) Pattern

According to the dominant site of fibrosis throughout the myocardium, five patterns were defined by visual assessment: minimal interstitial fibrosis (not restricted to one area of the biopsy), sub-endocardial, mid-wall, sub-epicardial and transmural fibrosis (Figure 2A).

III) Architecture

The dominant architecture of fibrosis present within a TB was defined as: interstitial, patchy, diffuse, compact or a combination thereof (for definitions and examples see Figure 2B). Pattern and architecture of fibrosis in a random selection of TB were reviewed by a co-author (C.B.) to assess inter-observer agreement (Supplementary data).

IV) Amount

Wall thickness (WT) of each TB was measured. Custom pixel-by-pixel software calculated the percentage of fibrosis and the amount of viable myocardium (mm^2) within each TB (Supplementary data). The area of viable myocardium was used as a surrogate for the volume of viable myocardium at that location (Supplementary data). From the control biopsies, 7μm sections were taken and the percentage fibrosis calculated.

Statistical analysis

Normally distributed data was reported as mean±standard deviation; not normally distributed data as median and interquartile range [IQR]. Categorical data was expressed as percentages or frequencies. Continuous variables were compared using (multivariable) linear regression analysis in a model that allowed for intragroup correlation. Statistical analysis was performed using IBM SPSS

version 23 (SPSS Inc., Chicago, IL.) or STATA Statistical Software (StataCorp, College Station, TX), version 14.

Results

Patients

EAVM data and whole heart histology of eight male NICM patients with MVT (median age 63 [IQR 58-68] years) were analysed (Table 1). Seven patients died and one patient was successfully transplanted a median of 25 [IQR 6-217] days after EAVM. Cause of death was sepsis (n=2) 28 and 497 days after ablation, cardiogenic shock and/or severe vasoplegia with multiorgan failure (n=4) within 5 days of ablation and in one case cardiogenic shock 21 days after ablation without VT or obvious luxation.

Electroanatomical voltage mapping

All eight patients underwent LV endocardial mapping. Five underwent combined endo-epicardial mapping (Supplementary data). In two patients, a second mapping procedure was performed within 29 days and data from both procedures were included.

Controls

Control tissue for histology was obtained from seven age-matched hearts (five male, median age 65 [IQR 59-67] years). From each heart, four LV transmural biopsies were taken from the anterior, lateral, inferior and septal walls. The amount of fibrosis in each biopsy was assessed, with a median of 6.5% [IQR 4.9-9.3] fibrosis. Based on the 95th percentile, 21% was defined as the upper limit of normal quantity of fibrosis for this age group.

Ex-vivo integration

Integration of the ex-vivo 3D meshes with the in-vivo mapping data was accurate based on good agreement between macroscopically or histologically identified ablation lesion and ablation sites on EAVM (figure 1D). A median of 138 [IQR 98-198] endocardial and 172 [IQR 142-338] epicardial mapping points per patient were included for analysis.

Histology of NICM

In total, 507 TB (56 [IQR 34-96] TB per patient) were taken; 277 corresponding to endocardial non-ablation EAVM sites (endocardial TB) and 230 corresponding to epicardial non-ablation EAVM sites (epicardial TB) (Supplementary data).

I) Location

On histological analysis, all NICM hearts showed pathological amounts of fibrosis. The basal-anterior and basal-septal segments were most frequently affected, followed by mid-anterior and apical-anteroseptal involvement. UV mapping overestimated and BV mapping underestimated involvement as derived from histology (Supplementary data).

II) Pattern

Of all TB, 32 (6%) were classified as having minimal interstitial fibrosis on visual assessment, 153 (30%) were classified as dominant sub-endocardial fibrosis, 96 (19%) as mid-wall, 83 (17%) as sub-epicardial, and 143 (28%) as transmural fibrosis.

III) Architecture

A patchy architecture was the most common dominant architecture and occurred in 277 (55%) of TB, followed by diffuse in 171 (34%) and interstitial in 45 (9%) (Supplementary data). Of interest, compact fibrosis was the dominant architecture in only 14 TB (3%) and never extended transmurally. In 457 TB (90%) a combination of two or three architectures was observed. The most common combination of fibrosis architecture was patchy and interstitial (44% of all TB).

IV) Amount

TB had a median WT of 13.8mm [IQR 9.8-17.5], 25% fibrosis [IQR 19.1-32.1], and 45.8mm^2 [IQR 32.5-59.7] viable myocardium. In total, 160 TB (32%) had normal amounts of fibrosis if matched for age.

Voltages and corresponding histology

Voltages and histological parameters of TB with normal and abnormal amounts of fibrosis are given in Table 2.

Voltages and ex-vivo wall thickness

Within TB with normal amounts of fibrosis, there was a linear relationship between WT and endocardial UV (Figure 3A). For every millimetre increase in ex-vivo WT the UV increased by 0.28mV (p=0.010). Of interest, the same linear relationship was observed between BV and WT: for every millimetre increase in ex-vivo WT the BV increased by 0.23mV (p=0.009).

Voltages and amount of viable myocardium

In all TB, a linear relationship between amount of viable myocardium and UV generated was observed. A 1mm^2 increase in viable myocardium resulted in a 0.09mV (p=0.002) increase in endocardial UV (Figure 3B) and a 0.08mV (p=0.016) increase in epicardial UV. Notably, there was a comparable linear relationship between amount of viable myocardium and the endocardial BV generated. A 1mm^2 increase in amount of viable myocardium resulted in a 0.06mV (p=0.001) increase in endocardial BV.

A single cut-off to detect an amount of viable myocardium performed poorly irrespective of the amount of viable myocardium that was considered relevant (Supplementary data).

Field of view of UV and BV

It has previously been suggested that BV is limited by a field of view[7, 16]. To test the impact of fibrosis remote from the endocardial surface, the relationship between amount of viable

myocardium within TB and the endocardial voltages generated was analysed within a sub-selection of TB which had a normal amount of fibrosis in the 4mm sub-endocardium (figure 3C). Both UV and BV were impacted by changes in the amount of viable myocardium occurring at distances of >4mm from the endocardial surface. A 1mm^2 increase in the amount of viable myocardium beyond the 4mm sub-endocardial rim resulted in a UV increase of 0.09mV ($p=0.012$) and BV increase of 0.05mV ($p=0.046$).

Voltages, ex-vivo wall thickness and amount of fibrosis

Multiple linear regression was performed to predict the amount of fibrosis based on the voltage and WT measured. Both UV and BV can be used to predict the amount of fibrosis when ex-vivo WT is known ($p\leq0.017$). An equation taking into account both WT and the amount of fibrosis present was generated (Figure 4).

Discussion

Main findings

This study is the first to provide detailed histological data on fibrosis in NICM patients with sustained MVT and to couple EAVM data with the true gold standard for fibrosis identification - histology. The fibrosis pattern is highly variable and not restricted to the mid-wall and sub-epicardium. The fibrosis architecture is most often patchy or diffuse and a combination of more than one architecture occurs frequently. The compact fibrosis architecture observed in infarct scar is very rare in NICM and never reaches transmurality.

UV, and contrary to most commonly held beliefs, BV, are affected by WT. Additionally, the amount of fibrosis affects UV and BV. We demonstrate a linear relationship between the amount of viable myocardium and both the UV and BV amplitudes (Summarizing Figure). In this patient population, neither BV nor UV are restricted by a "field of view".

Our findings have important clinical implications. Firstly, a single BV or UV cut-off to detect fibrosis, as currently applied in practice, cannot be valid considering the range of observed WT. Secondly, as the relationship between UV and BV amplitude and WT remains linear with increasing fibrosis, we may be able to determine the amount of intramural fibrosis if the local WT is known.

Fibrosis in NICM

The only histological data in patients with NICM come from dated autopsy studies in patients with terminal heart failure[17-19]. These studies showed a dominant sub-endocardial fibrosis pattern which may be attributed to pressure overload or ischemia. In end-stage heart failure patients a variable degree of interstitial fibrosis was seen at sites of induced focal, non-sustained, polymorphic VTs[20].

Late gadolinium enhanced cardiac magnetic resonance (LGE-CMR) is the imaging reference method for the non-invasive detection of regional fibrosis in NICM[21]. A study including 63 unselected patients with dilated cardiomyopathy reported no LGE in the majority of patients (59%), sub-endocardial LGE in 13% (attributed to ischemia) and mid-wall or sub-epicardial LGE in 28% typically involving the basal and mid LV[22]. The presence and extent of particularly mid-wall fibrosis has been associated with inducible VT[23] and with mortality and (aborted) sudden cardiac death in a recent cohort of 472 NICM patients[24].

Our study is the first to specifically describe the fibrosis pattern and architecture in patients with NICM and sustained MVT. In contrast to what is reported in imaging studies, the mid-wall or sub-epicardial fibrosis pattern was seen in only 36% of TB. A further 30% showed a sub-endocardial pattern and a transmural pattern was seen in 28%. Of importance, only 3% of TB showed compact fibrosis with the density of ischemic scars, and this fibrosis was never transmural. A patchy (55%), followed by a diffuse architecture (34%) was most frequently found.

To date, LGE-CMR to detect and determine scar size has only been histologically validated in an ex-vivo animal model for post-infarct scar[25]. Current LGE-CMR methods to detect fibrosis require either bright areas with dense fibrosis or normal reference myocardium. The present study

demonstrates that in NICM, areas with compact fibrosis are rare and that "normal" reference myocardium may contain variable degrees of fibrosis. The comparison of in-vivo LGE-CMR data from one patient obtained 133 days before mapping and ablation illustrates the variation in scar size dependent on the applied LGE-CMR method and supports the limitation of LGE-CMR to accurately identify and delineate diffuse fibrosis (Figure 5 and Supplementary data)[23, 26-28].

Voltage mapping in NICM

Voltage mapping is considered the gold standard for the invasive identification of fibrosis. The cut-off values for UV and BV proposed in the literature vary in their absolute value and in the population in which they were derived. Cut-offs UV>8.27mV and BV>1.5mV were derived from patients without structural heart disease. However, sampling locations and WT in these young patients were not reported and these cut-offs were poor predictors of normal amounts of fibrosis in our cohort (Supplementary data).

Ischemic cardiomyopathy studies (pig models and humans) have shown that BV<1.5mV is useful in identifying compact, transmural, thin walled scars. However, BV<1.5mV could not detect non-transmural, small sub-epicardial scar or gray-zone[26, 29]. This was attributed to the smaller field of view of BV and it has been suggested that cut-offs based on ischemic scars may not be valid for NICM scars[8, 9, 30].

Linear relationship between wall thickness and UV and BV amplitude

EAVM is considered an indirect measure of the amount of viable myocardium depolarized in the vicinity of the recording electrodes. The amplitude of an electrogram generated by activity in a myocardial bundle is inversely proportional to the square or cube of the distance between the myocardial bundle and the recording site for UV ($UV \propto 1/r^2$) and BV ($BV \propto 1/r^3$) (Supplementary data)[31]. As such, myocardial bundles located closer to the catheter contribute more to the amplitude of both UV and BV electrograms than myocardial bundles located further away from the catheter.

Additionally, BV is less sensitive to the activity of viable myocardium occurring at distances remote from the catheter tip than UV, leading to the concept of a limited "field of view"[7, 16].

Of interest, we found a linear relation between WT and electrogram amplitude for both UV and BV. Importantly, for relatively large distances between 10-20mm, the relationship between WT and amplitude is near linear (Supplementary data), which is in line with the linear relationship we found between BV and UV within the clinically relevant range of WT in our cohort.

Linear relationship between amount of fibrosis and UV and BV amplitude

Not only the WT, but also the amount of fibrosis, affects the amount of viable myocardium present and thus influences both UV and BV. An increase in fibrosis reduces the amount of viable myocardium resulting in a linear decrease in UV and BV. Our data demonstrated such a linear relationship. Accordingly, it is important to take both these parameters into account when interpreting EAVM data.

"Field of view" of UV and BV

In this study we show that both UV and BV are sensitive to histological changes occurring more distantly from the catheter tip. We could demonstrate that endocardial BV is also affected by fibrosis occurring >4mm from the catheter. Whether BV and UV amplitudes, as well as voltages generated using a catheter with smaller electrodes, provide complementary information on fibrosis location needs further evaluation. Smaller electrodes are likely to reduce far field contamination and may be beneficial for areas with sub-endocardial involvement but would be potentially less helpful in areas with a mid-wall pattern of fibrosis.

Conclusions

Fibrosis pattern in patients with NICM and VTs are variable with similar prevalence of sub-endocardial, mid-wall/sub-epicardial and transmural patterns. Patchy and diffuse architectures dominate whereas compact fibrosis is rare. These specific characteristics of fibrosis are likely to

impact its accurate delineation by current LGE-CMR methods. Both BV and UV mapping are sensitive not only to the amount of fibrosis but also to myocardial WT. Similarly, both BV and UV mapping are not restricted by a "field of view". Accordingly, and of high clinical importance, a single BV and UV cut-off for detecting the amount and location of fibrosis without considering the local WT and architecture of fibrosis cannot be valid.

This study has taken an important step in this regard, providing an equation for detection of fibrosis based on UV and/or BV and WT. Further study is needed to generate a comprehensive algorithm, appropriate for in-vivo, real time, mapping and imaging.

Limitations

Whilst we have described the fibrosis present in NICM patients with VT, the specific fibrosis needed to sustain VT has not been identified.

This study reported ex-vivo WT. WT measured in formalin-fixed hearts are comparable to the end-systolic WT measured on echocardiography[32].

One-sentence summary

For the first time, voltage mapping for substrate delineation in non-ischemic cardiomyopathy (NICM) has been validated by full human heart histology; the substrate present in NICM is fundamentally different from that in ischemic cardiomyopathy and the approach to voltage mapping (BV and UV) currently applied world-wide needs to be redefined to take fibrosis and also wall thickness into account.

References

1. Hsia HH, Callans DJ, Marchlinski FE. Characterization of endocardial electrophysiological substrate in patients with nonischemic cardiomyopathy and monomorphic ventricular tachycardia. Circulation 2003;**108**(6):704-10.
2. Soejima K, Stevenson WG, Sapp JL, Selwyn AP, Couper G, Epstein LM. Endocardial and epicardial radiofrequency ablation of ventricular tachycardia associated with dilated cardiomyopathy: the importance of low-voltage scars. J Am Coll Cardiol 2004;**43**(10):1834-42.
3. Morita N, Mandel WJ, Kobayashi Y, Karagueuzian HS. Cardiac fibrosis as a determinant of ventricular tachyarrhythmias. J Arrhythm 2014;**30**(6):389-394.
4. de Jong S, van Veen TA, van Rijen HV, de Bakker JM. Fibrosis and cardiac arrhythmias. J Cardiovasc Pharmacol 2011;**57**(6):630-8.
5. Kawara T, Derksen R, de Groot JR, Coronel R, Tasseron S, Linnenbank AC, Hauer RN, Kirkels H, Janse MJ, de Bakker JM. Activation delay after premature stimulation in chronically diseased human myocardium relates to the architecture of interstitial fibrosis. Circulation 2001;**104**(25):3069-75.
6. Priori SG, Blomstrom-Lundqvist C, Mazzanti A, Blom N, Borggrefe M, Camm J, Elliott PM, Fitzsimons D, Hatala R, Hindricks G, Kirchhof P, Kjeldsen K, Kuck KH, Hernandez-Madrid A, Nikolaou N, Norekval TM, Spaulding C, Van Veldhuisen DJ, Kolh P, Lip GYH, Agewall S, Baron-Esquivias G, Boriani G, Budts W, Bueno H, Capodanno D, Carerj S, Crespo-Leiro MG, Czerny M, Deaton C, Dobrev D, Erol C, Galderisi M, Gorenek B, Kriebel T, Lambiase P, Lancellotti P, Lane DA, Lang I, Manolis AJ, Morais J, Moreno J, Piepoli MF, Rutten FH, Sredniawa B, Zamorano JL, Zannad F, Cardiology ES. 2015 ESC Guidelines for the management of patients with ventricular arrhythmias and the prevention of sudden cardiac death The Task Force for the Management of Patients with Ventricular Arrhythmias and the Prevention of Sudden Cardiac Death of the European Society of Cardiology (ESC) Endorsed by: Association for European Paediatric and Congenital Cardiology (AEPC). European Heart Journal 2015;**36**(41):2793-+.
7. Hutchinson MD, Gerstenfeld EP, Desjardins B, Bala R, Riley MP, Garcia FC, Dixit S, Lin D, Tzou WS, Cooper JM, Verdino RJ, Callans DJ, Marchlinski FE. Endocardial unipolar voltage mapping to detect epicardial ventricular tachycardia substrate in patients with nonischemic left ventricular cardiomyopathy. Circ Arrhythm Electrophysiol 2011;**4**(1):49-55.
8. Desjardins B, Yokokawa M, Good E, Crawford T, Latchamsetty R, Jongnarangsin K, Ghanbari H, Oral H, Pelosi F, Jr., Chugh A, Morady F, Bogun F. Characteristics of intramural scar in patients with nonischemic cardiomyopathy and relation to intramural ventricular arrhythmias. Circ Arrhythm Electrophysiol 2013;**6**(5):891-7.
9. Piers SR, Tao Q, van Huls van Taxis CF, Schalij MJ, van der Geest RJ, Zeppenfeld K. Contrast-enhanced MRI-derived scar patterns and associated ventricular tachycardias in nonischemic cardiomyopathy: implications for the ablation strategy. Circ Arrhythm Electrophysiol 2013;**6**(5):875-83.
10. Campos B, Jauregui ME, Park KM, Mountantonakis SE, Gerstenfeld EP, Haqqani H, Garcia FC, Hutchinson MD, Callans DJ, Dixit S, Lin D, Riley MP, Tzou W, Cooper JM, Bala R, Zado ES, Marchlinski FE. New unipolar electrogram criteria to identify irreversibility of nonischemic left ventricular cardiomyopathy. J Am Coll Cardiol 2012;**60**(21):2194-204.
11. Desjardins B, Morady F, Bogun F. Effect of epicardial fat on electroanatomical mapping and epicardial catheter ablation. J Am Coll Cardiol 2010;**56**(16):1320-7.
12. Reddy VY, Malchano ZJ, Holmvang G, Schmidt EJ, d'Avila A, Houghtaling C, Chan RC, Ruskin JN. Integration of cardiac magnetic resonance imaging with three-dimensional electroanatomic

mapping to guide left ventricular catheter manipulation: feasibility in a porcine model of healed myocardial infarction. J Am Coll Cardiol 2004;**44**(11):2202-13.
13. de Bakker JM, van Capelle FJ, Janse MJ, Wilde AA, Coronel R, Becker AE, Dingemans KP, van Hemel NM, Hauer RN. Reentry as a cause of ventricular tachycardia in patients with chronic ischemic heart disease: electrophysiologic and anatomic correlation. Circulation 1988;**77**(3):589-606.
14. Marchlinski FE, Callans DJ, Gottlieb CD, Zado E. Linear ablation lesions for control of unmappable ventricular tachycardia in patients with ischemic and nonischemic cardiomyopathy. Circulation 2000;**101**(11):1288-96.
15. Piers SR, van Huls van Taxis CF, Tao Q, van der Geest RJ, Askar SF, Siebelink HM, Schalij MJ, Zeppenfeld K. Epicardial substrate mapping for ventricular tachycardia ablation in patients with non-ischaemic cardiomyopathy: a new algorithm to differentiate between scar and viable myocardium developed by simultaneous integration of computed tomography and contrast-enhanced magnetic resonance imaging. Eur Heart J 2013;**34**(8):586-96.
16. Haqqani HM, Tschabrunn CM, Tzou WS, Dixit S, Cooper JM, Riley MP, Lin D, Hutchinson MD, Garcia FC, Bala R, Verdino RJ, Callans DJ, Gerstenfeld EP, Zado ES, Marchlinski FE. Isolated septal substrate for ventricular tachycardia in nonischemic dilated cardiomyopathy: incidence, characterization, and implications. Heart Rhythm 2011;**8**(8):1169-76.
17. Roberts WC, Siegel RJ, McManus BM. Idiopathic dilated cardiomyopathy: analysis of 152 necropsy patients. Am J Cardiol 1987;**60**(16):1340-55.
18. Unverferth DV, Baker PB, Swift SE, Chaffee R, Fetters JK, Uretsky BF, Thompson ME, Leier CV. Extent of myocardial fibrosis and cellular hypertrophy in dilated cardiomyopathy. Am J Cardiol 1986;**57**(10):816-20.
19. de Leeuw N, Ruiter DJ, Balk AH, de Jonge N, Melchers WJ, Galama JM. Histopathologic findings in explanted heart tissue from patients with end-stage idiopathic dilated cardiomyopathy. Transpl Int 2001;**14**(5):299-306.
20. Pogwizd SM, McKenzie JP, Cain ME. Mechanisms underlying spontaneous and induced ventricular arrhythmias in patients with idiopathic dilated cardiomyopathy. Circulation 1998;**98**(22):2404-14.
21. Iles LM, Ellims AH, Llewellyn H, Hare JL, Kaye DM, McLean CA, Taylor AJ. Histological validation of cardiac magnetic resonance analysis of regional and diffuse interstitial myocardial fibrosis. Eur Heart J Cardiovasc Imaging 2015;**16**(1):14-22.
22. McCrohon JA, Moon JC, Prasad SK, McKenna WJ, Lorenz CH, Coats AJ, Pennell DJ. Differentiation of heart failure related to dilated cardiomyopathy and coronary artery disease using gadolinium-enhanced cardiovascular magnetic resonance. Circulation 2003;**108**(1):54-9.
23. Nazarian S, Bluemke DA, Lardo AC, Zviman MM, Watkins SP, Dickfeld TL, Meininger GR, Roguin A, Calkins H, Tomaselli GF, Weiss RG, Berger RD, Lima JA, Halperin HR. Magnetic resonance assessment of the substrate for inducible ventricular tachycardia in nonischemic cardiomyopathy. Circulation 2005;**112**(18):2821-5.
24. Gulati A, Jabbour A, Ismail TF, Guha K, Khwaja J, Raza S, Morarji K, Brown TD, Ismail NA, Dweck MR, Di Pietro E, Roughton M, Wage R, Daryani Y, O'Hanlon R, Sheppard MN, Alpendurada F, Lyon AR, Cook SA, Cowie MR, Assomull RG, Pennell DJ, Prasad SK. Association of fibrosis with mortality and sudden cardiac death in patients with nonischemic dilated cardiomyopathy. JAMA 2013;**309**(9):896-908.
25. Fieno DS, Kim RJ, Chen EL, Lomasney JW, Klocke FJ, Judd RM. Contrast-enhanced magnetic resonance imaging of myocardium at risk: distinction between reversible and irreversible injury throughout infarct healing. J Am Coll Cardiol 2000;**36**(6):1985-91.
26. Wijnmaalen AP, van der Geest RJ, van Huls van Taxis CF, Siebelink HM, Kroft LJ, Bax JJ, Reiber JH, Schalij MJ, Zeppenfeld K. Head-to-head comparison of contrast-enhanced magnetic resonance imaging and electroanatomical voltage mapping to assess post-infarct scar characteristics in patients with ventricular tachycardias: real-time image integration and reversed registration. Eur Heart J 2011;**32**(1):104-14.

27. Schmidt A, Azevedo CF, Cheng A, Gupta SN, Bluemke DA, Foo TK, Gerstenblith G, Weiss RG, Marban E, Tomaselli GF, Lima JA, Wu KC. Infarct tissue heterogeneity by magnetic resonance imaging identifies enhanced cardiac arrhythmia susceptibility in patients with left ventricular dysfunction. Circulation 2007;**115**(15):2006-14.
28. Yan AT, Shayne AJ, Brown KA, Gupta SN, Chan CW, Luu TM, Di Carli MF, Reynolds HG, Stevenson WG, Kwong RY. Characterization of the peri-infarct zone by contrast-enhanced cardiac magnetic resonance imaging is a powerful predictor of post-myocardial infarction mortality. Circulation 2006;**114**(1):32-9.
29. Wrobleski D, Houghtaling C, Josephson ME, Ruskin JN, Reddy VY. Use of electrogram characteristics during sinus rhythm to delineate the endocardial scar in a porcine model of healed myocardial infarction. J Cardiovasc Electrophysiol 2003;**14**(5):524-9.
30. Sasaki T, Miller CF, Hansford R, Zipunnikov V, Zviman MM, Marine JE, Spragg D, Cheng A, Tandri H, Sinha S, Kolandaivelu A, Zimmerman SL, Bluemke DA, Tomaselli GF, Berger RD, Halperin HR, Calkins H, Nazarian S. Impact of nonischemic scar features on local ventricular electrograms and scar-related ventricular tachycardia circuits in patients with nonischemic cardiomyopathy. Circ Arrhythm Electrophysiol 2013;**6**(6):1139-47.
31. Durrer D, Van Der Twell LH. Spread of activation in the left ventricular wall of the dog. I. Am Heart J 1953;**46**(5):683-91.
32. Maron BJ, Henry WL, Roberts WC, Epstein SE. Comparison of echocardiographic and necropsy measurements of ventricular wall thicknesses in patients with and without disproportionate septal thickening. Circulation 1977;**55**(2):341-6.

Figure Legends

Figure 1

A. Endocardial and epicardial BV maps, color-coded according to bar in an anterior-posterior view. B Creation of 3D-mesh from 5mm pathological slices. C. Integration of voltage maps with 3D anatomical mesh (grey). D. Example of four slices with EAVM points and ablation locations projected. Accurate integration confirmation by visual inspection of projection of ablation locations over pathology ablation lesions. EAVM mapping locations (a-h) shown on CARTO maps and on histological slices. Stained 5mm wide biopsy corresponding to non-ablation site A. Collagen stains red, myocardium yellow.

Figure 2

A. Patterns of fibrosis.

B. Architecture of fibrosis. Interstitial: fibrosis in the extracellular space between myocardial bundles; patchy: areas of replacement fibrosis, surrounded by confluent viable myocardium; diffuse: intermingling of myocardial and collagen fibres; compact: dense areas of fibrosis, spanning the full width of the TB devoid of any viable myocardium.

C. Custom software used to calculate the amount of fibrosis.

Figure 3

A. WT and voltages in TB with normal amounts of fibrosis. B. Viable myocardium and corresponding voltages. The 1.5mV and 8.27mV mark indicate clinically applied cut-off values. C. TB with <21% in the 4mm sub-endocardial rim (n=79): UV and BV against viable myocardium within the entire biopsy.

Figure 4

A. Equations to predict amount of fibrosis when WT (mm) and voltages (mV) are known. B. Voltages (mV) generated when ex-vivo WT (mm) and % fibrosis are known.

Figure 5

Red dotted line: ICD artefact. Red: scar core. Yellow: scar borderzone according to different methods (Supplementary data). Green squares: locations of high-resolution histology inserts from non-ablation locations. Areas of dense mid-septal fibrosis surrounded by viable myocardium corresponded well with areas of LGE on CMR (insert 2). Despite high quantity, less well delineated fibrosis (insert 1) was only identified as core scar when using the 2-3SD method; as borderzone when using the Max_{SI} or modified FWHM method. Despite comprising more than 50% fibrosis, a diffuse pattern was not detected on LGE-CMR irrespective of method used (insert 3).

Text Tables

Table 1.

Baseline characteristics	
Male (%)	8 (100%)
Age, years	63 [58-65]
Co-morbidity*	4 (50%)
Family history of SCD	2 (25%)
ICD	7 (87.5%)
Genetic testing performed	8 (100%)
Pathogenic mutation†	5 (63%)
Unclassified variant‡	1 (13%)
Clinical presentation	
LVEF (%)	35 [20-43]
VT storm/incessant VT	6 (75%)
Prior ablation in different centre	3 (38%)
Amiodarone use	8 (100%)
Escalation of AAD	5 (63%)

Legend: *Renal disease, COPD, Diabetes Mellitus. †ABCC9, TTN, Lamine A/C, RBM20, MYBPC-3; ‡MYH7. Escalation of AAD: amiodarone plus ≥1 class 1 anti-arrhythmic drug.

Table 2.

	All biopsies (n=507)	Endocardial biopsies (n=277)			Epicardial biopsies (n=230)		
		All biopsies (n=277)	<21% fibrosis (n=78)	>21% fibrosis (n=199)	All biopsies (n=230)	<21% fibrosis (n=82)	>21% fibrosis (n=148)
Fibrosis (%)	24.8 [19.1-32.1]	25.5 [20.1-33.7]	15.7 [9.3-18.8]	30.0 [24.6-37.8]	23.9 [18.7-30.6]	17.0 [13.7-18.8]	28.2 [24.4-34.1]
Wall thickness (mm)	13.8 [9.8-17.5]	14.4 [10.7-17.3]	15.1 [11.5-18.5]	14.0 [10.0-17.0]	13.2 [9.0-17.8]	14.8 [9.1-17.5]	12.8 [9.0-17.9]
Viable myocardium (mm^2)	45.8 [32.5-59.7]	46.8 [33.5-59.6]	60.0 [43.3-73.7]	42.1 [31.6-55.8]	45.1 [31.8-59.9]	54.5 [33.6-66.6]	40.8 [29.6-57.4]
Bipolar voltage (mV)	2.7[1.3-4.1]	2.6 [1.6-4.3]	3.3 [1.8-6.7]	2.4 [1.4-4.0]	2.7 [0.9-4.0]	3.4 [2.3-5.5]	1.8 [0.8-3.5]
Unipolar voltage (mV)	6.5 [4.5-9.2]	6.2 [4.5-9.0]	8.3 [5.9-10.9]	5.4 [4.3-8.1]	6.9 [4.6-9.3]	8.6 [6.6-11.9]	5.9 [4.1-8.1]
Epicardial fat (mm)		n.a.	n.a.	n.a.	0.5 [0.0-2.0]	0.2 [0.0-1.5]	0.6 [0.0-2.4]

Legend: Histological and voltage parameters of all biopsies, and biopsies subdivided based on location of voltage data (endocardial and epicardial) and on quantity of fibrosis (normal (<21%), abnormal (>21%)). Data given as median [IQR].

Figures

Summarizing Figure

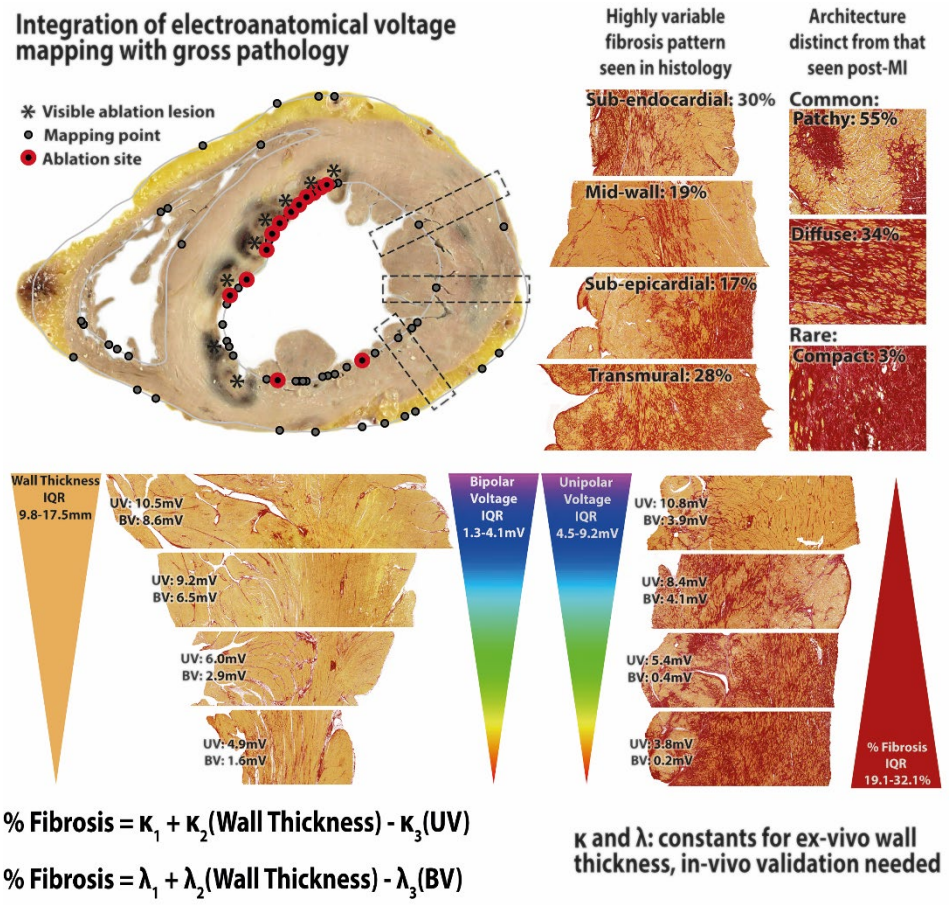

Figure 1.

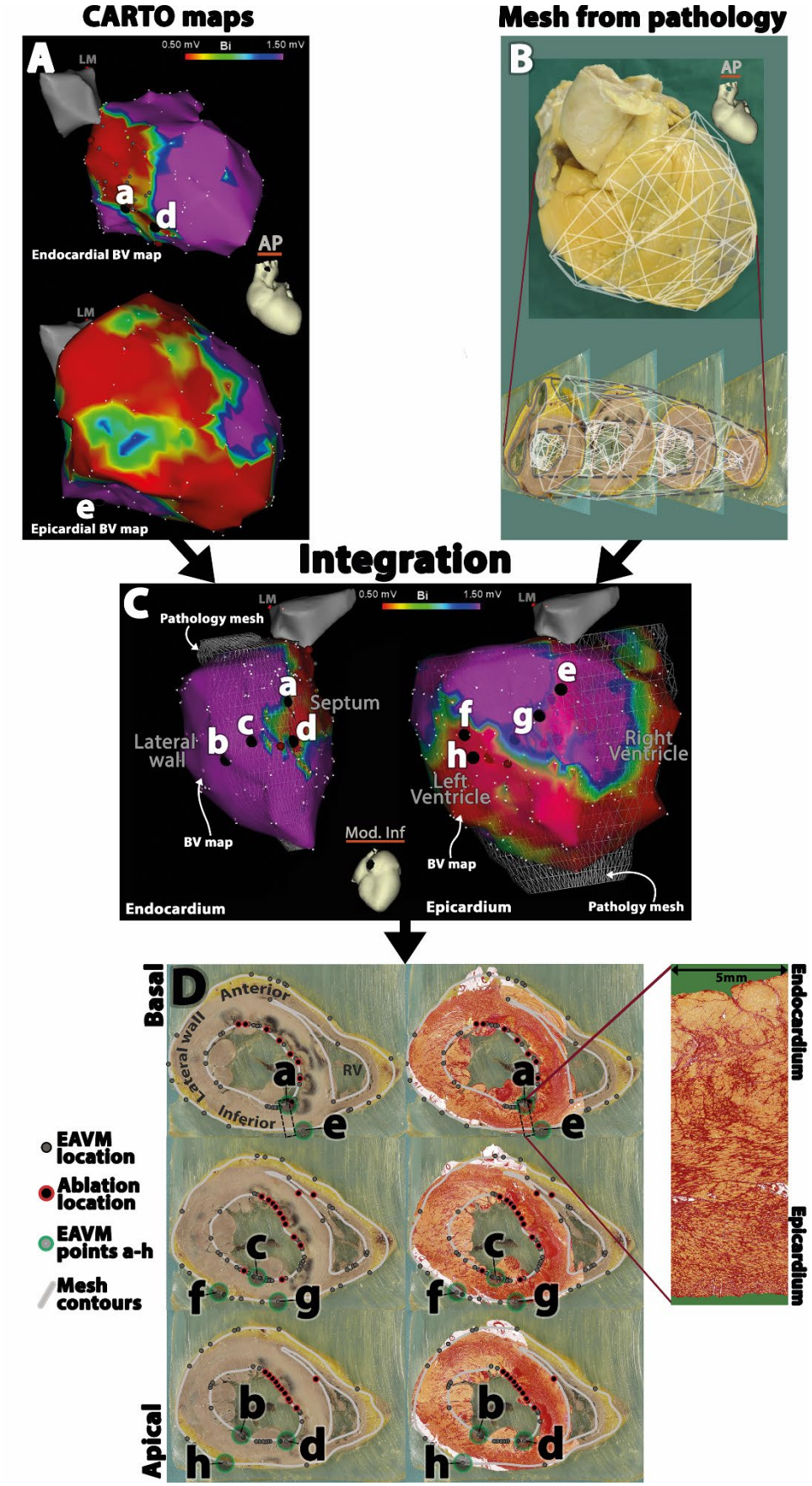
CARTO maps
Mesh from pathology
A
0.50 mV
Bi
1.50 mV
LM
a
d
Endocardial BV map
AP
LM
e
Epicardial BV map
B
AP
Integration
C
LM
0.50 mV
Bi
1.50 mV
LM
Pathology mesh
a
Septum
b
c
d
Lateral wall
BV map
Mod. Inf
e
f
g
h
Right Ventricle
Left Ventricle
BV map
Endocardium
Epicardium
Patholgy mesh
D
Basal
Anterior
Lateral wall
RV
Inferior
a
e
c
f
g
b
d
h
Apical
EAVM location
Ablation location
EAVM points a-h
Mesh contours
5mm
Endocardium
Epicardium

Figure 2.

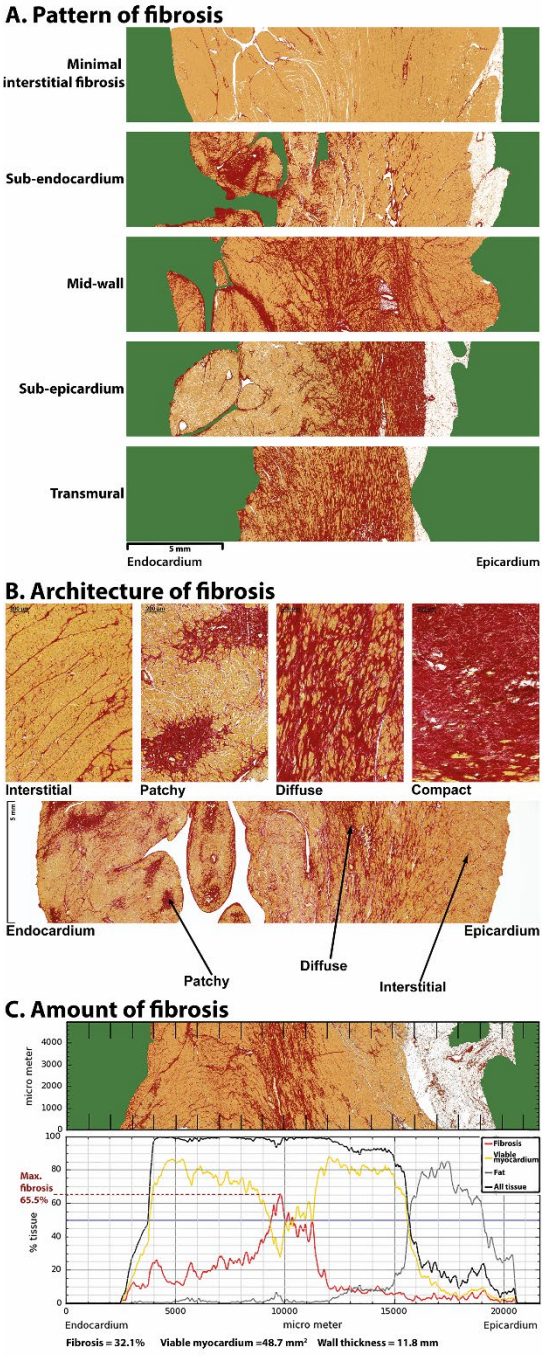
A. Pattern of fibrosis
Minimal interstitial fibrosis
Sub-endocardium
Mid-wall
Sub-epicardium
Transmural
5 mm
Endocardium
Epicardium
B. Architecture of fibrosis
Interstitial
Patchy
Diffuse
Compact
5 mm
Endocardium
Epicardium
Patchy
Diffuse
Interstitial
C. Amount of fibrosis
micro meter
4000
3000
2000
1000
0
100
80
60
40
20
0
% tissue
Max. fibrosis 65.5%
Fibrosis
Viable myocardium
Fat
All tissue
0
5000
10000
15000
20000
Endocardium
micro meter
Epicardium
Fibrosis = 32.1%
Viable myocardium =48.7 mm²
Wall thickness = 11.8 mm

Figure 3.

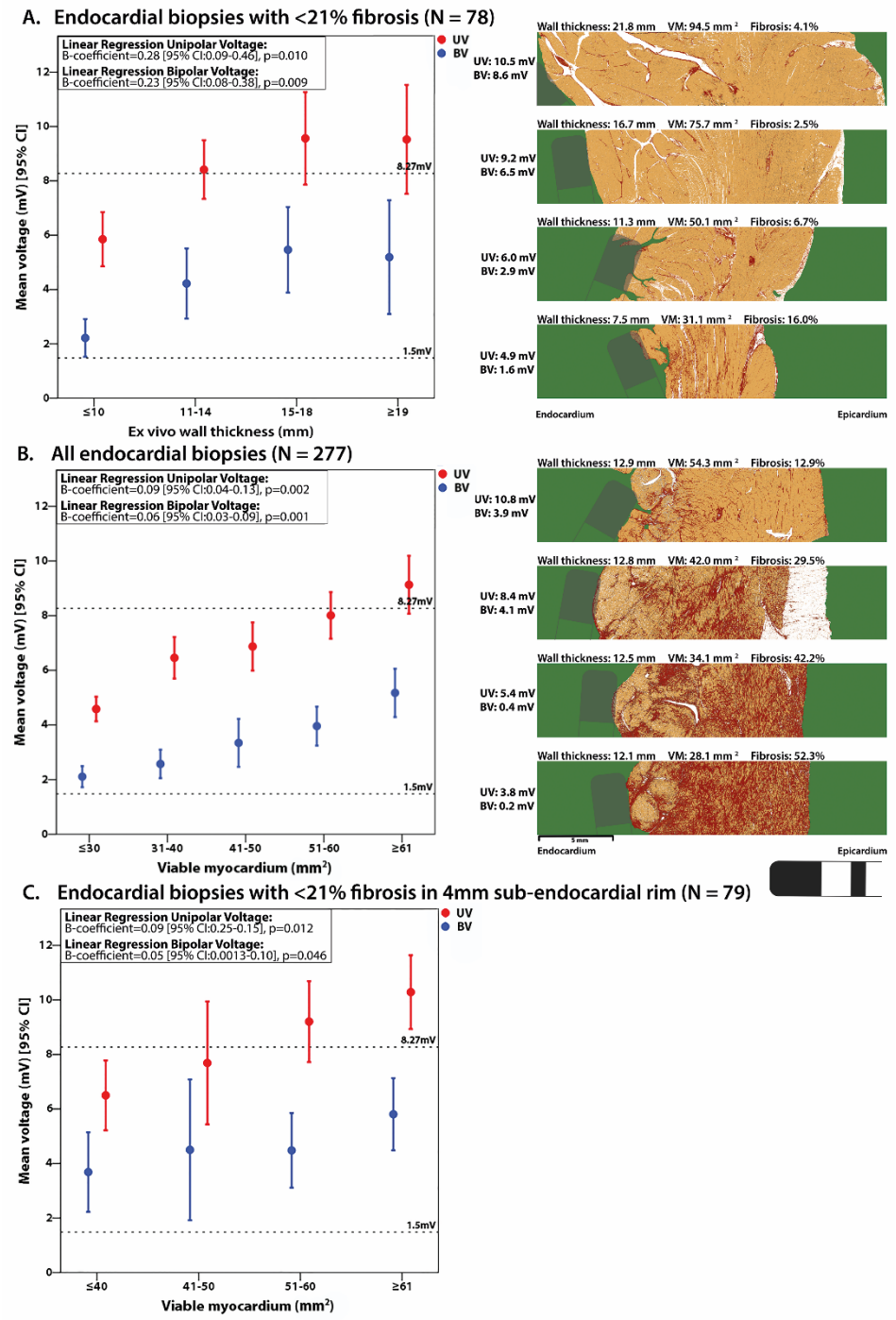
A. Endocardial biopsies with <21% fibrosis (N = 78)
Linear Regression Unipolar Voltage:
B-coefficient=0.28 [95% CI:0.09-0.46], p=0.010
Linear Regression Bipolar Voltage:
B-coefficient=0.23 [95% CI:0.08-0.38], p=0.009
UV
BV
Mean voltage (mV) [95% CI]
8.27mV
1.5mV
≤10
11-14
15-18
≥19
Ex vivo wall thickness (mm)
Wall thickness: 21.8 mm VM: 94.5 mm² Fibrosis: 4.1%
UV: 10.5 mV
BV: 8.6 mV
Wall thickness: 16.7 mm VM: 75.7 mm² Fibrosis: 2.5%
UV: 9.2 mV
BV: 6.5 mV
Wall thickness: 11.3 mm VM: 50.1 mm² Fibrosis: 6.7%
UV: 6.0 mV
BV: 2.9 mV
Wall thickness: 7.5 mm VM: 31.1 mm² Fibrosis: 16.0%
UV: 4.9 mV
BV: 1.6 mV
Endocardium
Epicardium
B. All endocardial biopsies (N = 277)
Linear Regression Unipolar Voltage:
B-coefficient=0.09 [95% CI:0.04-0.13], p=0.002
Linear Regression Bipolar Voltage:
B-coefficient=0.06 [95% CI:0.03-0.09], p=0.001
UV
BV
Mean voltage (mV) [95% CI]
8.27mV
1.5mV
≤30
31-40
41-50
51-60
≥61
Viable myocardium (mm²)
Wall thickness: 12.9 mm VM: 54.3 mm² Fibrosis: 12.9%
UV: 10.8 mV
BV: 3.9 mV
Wall thickness: 12.8 mm VM: 42.0 mm² Fibrosis: 29.5%
UV: 8.4 mV
BV: 4.1 mV
Wall thickness: 12.5 mm VM: 34.1 mm² Fibrosis: 42.2%
UV: 5.4 mV
BV: 0.4 mV
Wall thickness: 12.1 mm VM: 28.1 mm² Fibrosis: 52.3%
UV: 3.8 mV
BV: 0.2 mV
5 mm
Endocardium
Epicardium
C. Endocardial biopsies with <21% fibrosis in 4mm sub-endocardial rim (N = 79)
Linear Regression Unipolar Voltage:
B-coefficient=0.09 [95% CI:0.25-0.15], p=0.012
Linear Regression Bipolar Voltage:
B-coefficient=0.05 [95% CI:0.0013-0.10], p=0.046
UV
BV
Mean voltage (mV) [95% CI]
8.27mV
1.5mV
≤40
41-50
51-60
≥61
Viable myocardium (mm²)

Figure 4.

A

% fibrosis = 78.17 + 4.67(ex-vivo wall thickness) - 16.67(UV)

% fibrosis = 44 + 3.6(ex-vivo wall thickness) - 20(BV)

B

Fibrosis (%)	BV \ UV	Ex-vivo wall thickness (mm) 10	13	16	19
	15	6.6 / 3.3	7.5 / 3.8	8.3 / 4.4	9.1 / 4.9
	25	6.1 / 2.8	6.9 / 3.4	7.7 / 3.9	8.6 / 4.5
	35	5.5 / 2.4	6.4 / 2.9	7.2 / 3.5	8.0 / 4.0
	45	5.0 / 1.9	5.8 / 2.5	6.6 / 3.0	7.5 / 3.5

Figure 5.

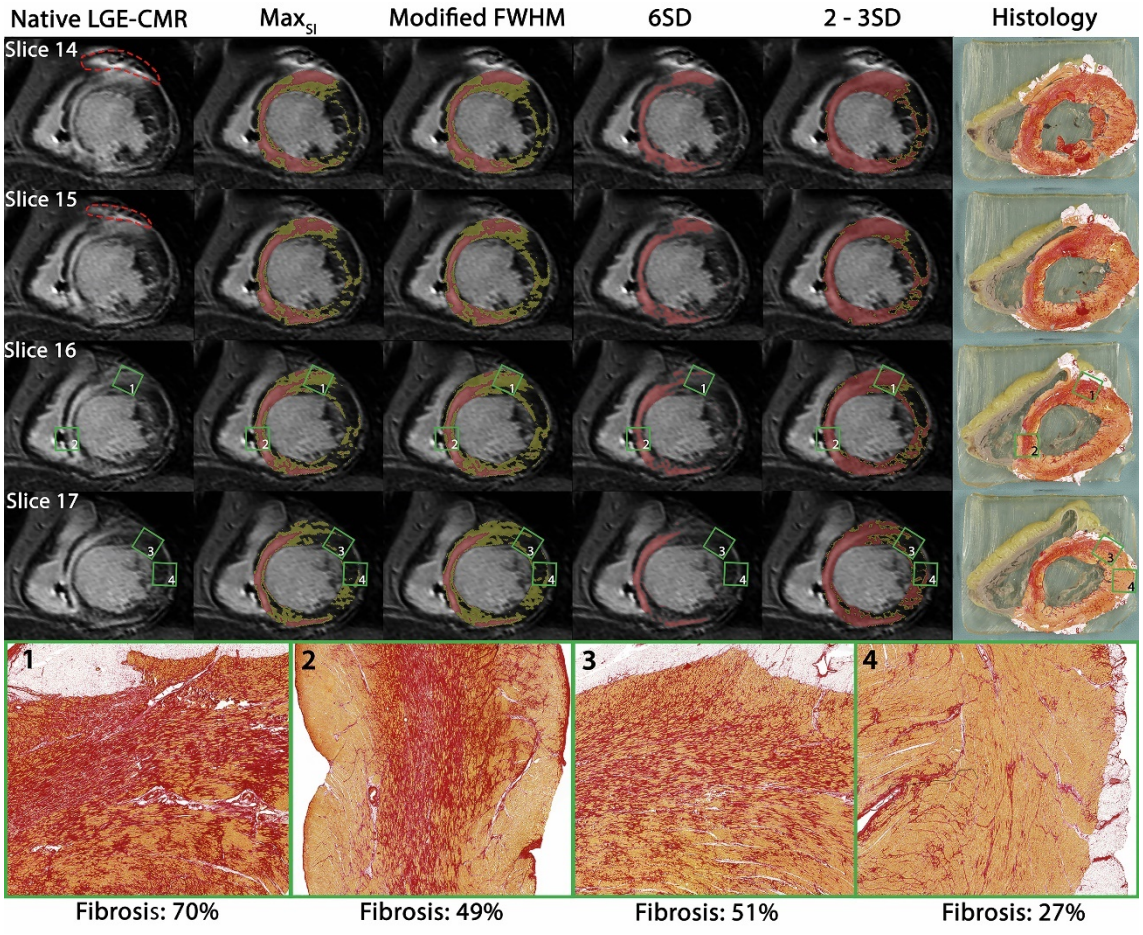
Native LGE-CMR
Max$_{SI}$
Modified FWHM
6SD
2 - 3SD
Histology
Slice 14
Slice 15
Slice 16
Slice 17
1
2
3
4
Fibrosis: 70%
Fibrosis: 49%
Fibrosis: 51%
Fibrosis: 27%

Funding

The Department of Cardiology (Leiden University Medical Centre) receives unrestricted research grant from Edwards Lifesciences, Medtronik, Biotronik, and Boston Scientific.

Conflict of Interest

None declared.